The ^{14}N Nuclear Quadrupole Coupling Tensors, the Tensors of the Molecular Magnetic Susceptibility and the Molecular Electric Quadrupole Moment in Pyrazole: A High Resolution Rotational Zeeman Effect Study

O. Böttcher and D. H. Sutter

Abteilung Chemische Physik im Institut für Physikalische Chemie der Christian Albrechts Universität zu Kiel, Kiel, West-Germany

Z. Naturforsch. **45a**, 1248–1258 (1990); received August 20, 1990

High resolution zero field and Zeeman rotational spectra of 1 D-pyrazole have been studied by microwave Fourier-transform spectroscopy. The zero field hfs patterns allowed to improve the quadrupole coupling constants for both ^{14}N nuclei. From the high field Zeeman multiplets the diagonal elements of the g-tensor were obtained as $g_{aa} = -0.1178(2)$,. $g_{bb} = -0.0762(2)$ and $g_{cc} = 0.0608(2)$. The two independent components of the molecular magnetic susceptibility anisotropy in units of 10^{-6} erg G^{-2} mole^{-1} are $2\xi_{aa} - \xi_{bb} - \xi_{cc} = 52.69(32)$ and $2\xi_{bb} - \xi_{cc} - \xi_{aa} = 39.32(29)$ were, a, b, c denote the molecular principal inertia axes. From these values the components of the molecular electric quadrupole moment tensor in units of 10^{-26} esu cm^2 follow as $Q_{aa} = 5.84(22)$, $Q_{bb} = -0.58$ (21) and $Q_{cc} = -5.27(38)$. Comparison with corresponding values for the undeuterated species leads to the complete tensors including their orientation with respect to the nuclear frame.

Introduction

The microwave spectrum of pyrazole ($C_3H_4N_2$) has been studied first by Kirchhoff [1]. Subsequent studies by Blackman et al. [2, 3] and Nygaard et al. [4] did lead to the ^{14}N quadrupole coupling constants and to a complete r_s-structure determination. The rotational Zeeman effect of the parent species has been studied by Stolze and Sutter [5]. From the present study ^{14}N quadrupole coupling constants were obtained for 1 D-pyrazole with considerably reduced experimental uncertainties. Also obtained were the diagonal elements of the molecular g-tensor and the molecular magnetic anisotropies. The changes in the aa-, bb- and cc-tensor elements upon deuteration, which are essentially caused by the rotation of the principal inertia axes system with respect to the nuclear frame, also made it possible to determine the tensors completely. High resolution is a prerequisite for such a study. It was achieved with the time domain Zeeman spectrometer developed recently at our laboratory [6, 7]. To our knowledge our present study is the second * in which the spectroscopic determination of the complete tensors of the molecular electric quadrupole moment and of the molecular magnetic susceptibility was carried out successfully for an asymmetric top molecule. Where possible the experimental values are compared with Hartree-Fock SCF-results calculated at the r_s-structure.

Reprint requests to Prof. Dr. D. H. Sutter, Institut für Physikalische Chemie, Abtl. Chemische Physik, Christian Albrechts Universität, Ludewig-Mayn-Str. 8, 2300 Kiel, West-Germany.

* HNO_3: studied recently by Spiekermann and Albinus from our group, was the first molecule whose tensors were determined that way [8].

Experimental Details

The parent spezies, pyrazole, was purchased from EGA-Chemie, Weinheim, and was purified by vacuum sublimation. Due to the acidity of the pyrrolic hydrogen, 1 D-pyrazole was easily prepared in an exchange reaction with an excess of deuterated methanole. The isotopic mixture of methanole was distilled off in high vacuum. 1 D-pyrazole was sublimized into the absorption cell. Due to the low vapour pressure of pyrazole, the absorption cell was kept at room temperature. Typical sample pressures were close to 1 mTorr.

The spectra were taken with our new microwave Fourier-transform spectrometer described in [6]. In this spectrometer the molecules are coherently driven into non-eigenstates by short intense near-resonant microwave pulses. The subsequent transient emission signal is heterodyned down to an intermediate frequency in the MHz range and is sampled every 10 ns with a 1-bit analog to digital converter. Typically 1024 to 4096 subsequent data points are taken for each

0932-0784 / 90 / 1100-1248 $ 01.30/0. – Please order a reprint rather than making your own copy

Dieses Werk wurde im Jahr 2013 vom Verlag Zeitschrift für Naturforschung in Zusammenarbeit mit der Max-Planck-Gesellschaft zur Förderung der Wissenschaften e.V. digitalisiert und unter folgender Lizenz veröffentlicht: Creative Commons Namensnennung-Keine Bearbeitung 3.0 Deutschland Lizenz.

This work has been digitalized and published in 2013 by Verlag Zeitschrift für Naturforschung in cooperation with the Max Planck Society for the Advancement of Science under a Creative Commons Attribution-NoDerivs 3.0 Germany License.

Zum 01.01.2015 ist eine Anpassung der Lizenzbedingungen (Entfall der Creative Commons Lizenzbedingung „Keine Bearbeitung") beabsichtigt, um eine Nachnutzung auch im Rahmen zukünftiger wissenschaftlicher Nutzungsformen zu ermöglichen.

On 01.01.2015 it is planned to change the License Conditions (the removal of the Creative Commons License condition "no derivative works"). This is to allow reuse in the area of future scientific usage.

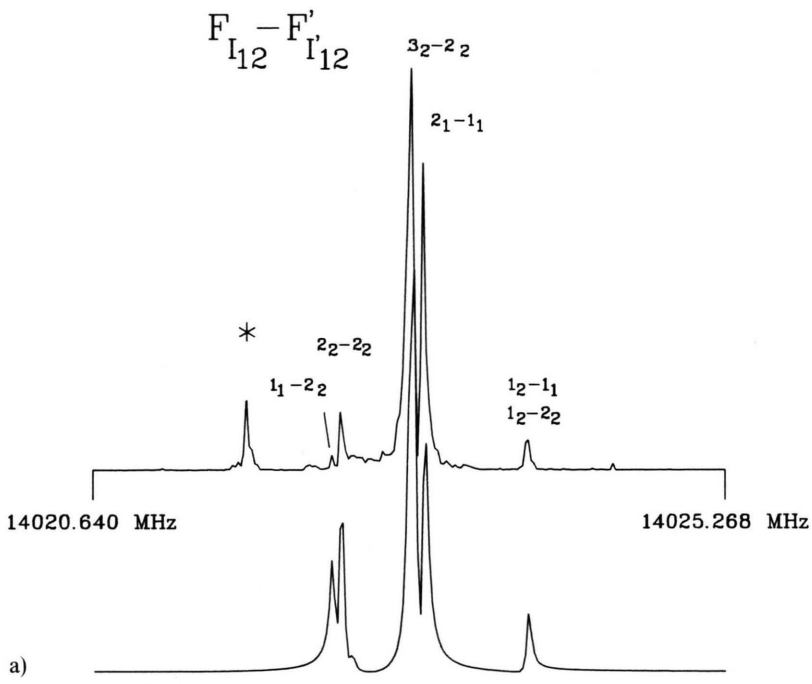

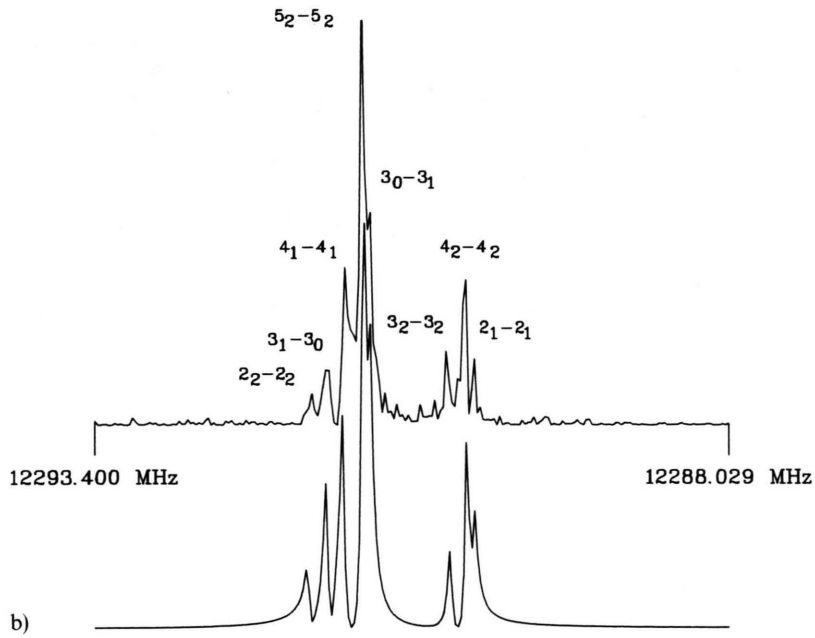

Fig. 1. Fourier transform power spectra of the transient emissions from the ^{14}N quadrupole hfs patterns of the a) $1_{11}-0_{00}$ and b) $3_{12}-3_{21}$ rotational transition of 1 D-pyrazole. The lower traces show simulations calculated within the high power/short pulse approximation. The quadrupole coupling constants given in Table 3 were used in the simulations. From the differences it is obvious that the short pulse approximation does not perfectly apply and that the polarization of each satellite signal actually depends on its off-resonance with respect to the polarizing microwave. The asterisk in a) indicates a signal from an unassigned transition which does not belong the hfs-pattern.

The experimental conditions were:
Sample pressures: a), b) 2 mTorr,
pulse lengths: a), b) 100 ns,
sample intervalls: a), b) 10 ns,
temperature: a), b) 298 K,
delays: a) 900 ns, b) 2000 ns,
data points: a), b) 4096.

transient decay and about 10^6 decays are averaged up prior to the analysis. The basic principles of 1-bit averaging of noisy signals have been discussed in detail in the Appendix of [9]. For a recent review on time domain microwave spectroscopy we refer to an article by Dreizler [10].

To derive the molecular resonance frequencies etc. from the observed transient emission signals, a two step analysis was carried out. In the first step a discrete Fourier-transform analysis was performed to obtain approximate values for the frequencies, initial amplitudes, phases and decay times hidden in the transient signal. Then these were taken as initial values for an iterative least square fit of the frequencies etc. to the observed decays [11]. As an illustration we present zero field ^{14}N-hfs patterns of the $1_{11}\rightarrow 0_{00}$ and $3_{12}\rightarrow 3_{21}$ transitions of 1 D-pyrazole in Figure 1. For the Zeeman studies the absorption cells were placed into the homogeneous central part of the field of a powerful electromagnet [6]. The electric dipole selection rules were chosen by the orientation of the cross section of the waveguide with respect to the magnetic field (compare ref. [12], p. 135). The field was measured with a Rawson Lush rotating coil gaussmeter type 920 M. The experimental uncertainties in the magnetic field strengths are determined by the small fluctuations of the current stabilized power supply. Over a measuring period of 1 hour and at a field of 20 kG (=2 Tesla) these fluctuations were typically less than ± 5G.

Table 1. Zero field ^{14}N quadrupole hfs multiplets observed for 1 D-pyrazole. F, F': quantum number of the overall angular momentum, $F=I_{12}+J$; I_{12}, I'_{12}: quantum number of the intermediate spin, $I_{12}=I_1+I_2$; ν_{exp}: experimental splitting with respect to the hypothetical center frequency (ν_{center}); ν_{calc}: splitting calculated with the optimized quadrupole coupling constants (compare Table 3); $\delta\nu$: $\nu_{exp}-\nu_{calc}$. Intensity: relative intensity of the satellite as it would be observed in a CW-spectrometer.

F	I_{12}	F'	I'_{12}	Frequency (MHz)			Intensity %
				ν_{exp}	ν_{calc}	$\delta\nu$	
$J_{K_a K_c}\rightarrow J'_{K_{a'} K_{c'}}$: $1_{11}\rightarrow 0_{00}$; ν_{center}: 14 028.025(8) MHz							
0	1	1	1	0.433	0.436	−0.003	3.8
1	0	0	0	−0.047	−0.052	0.005	8.0
1	0	1	1	−0.047	−0.052	0.005	3.1
1	1	0	0	0.582	0.597	−0.015	2.4
1	1	1	1	0.582	0.597	−0.015	3.8
1	1	2	2	0.582	0.597	−0.015	5.0
1	2	1	1	−1.076	−1.068	−0.008	4.3
1	2	2	2	−1.076	−1.068	−0.008	6.1
2	1	1	1	−0.187	−0.175	−0.012	13.0
2	1	2	2	−0.187	−0.175	−0.012	5.7
2	2	1	1	0.516	0.524	−0.008	5.7
2	2	2	2	0.516	0.524	−0.008	13.0
3	2	2	2	−0.081	−0.087	0.006	26.2
$J_{K_a K_c}\rightarrow J'_{K_{a'} K_{c'}}$: $3_{21}\rightarrow 3_{12}$; ν_{center}: 12 290.969(6) MHz							
1	2	1	2	0.403	0.405	−0.002	4.0
2	1	2	1	−0.751	−0.753	0.002	7.4
2	2	2	2	0.638	0.652	−0.014	6.2
3	0	3	1	0.125	0.125	0.000	12.2
3	1	3	0	0.496	0.495	0.001	11.0
3	2	3	2	−0.550	−0.552	0.002	9.8
4	1	4	1	0.343	0.360	−0.017	15.2
4	2	4	2	−0.687	−0.698	0.011	14.2
5	2	5	2	0.175	0.169	0.006	19.9

Analysis of the Zero Field and Zeeman Hyperfine Multiplets

The hfs multiplets of the $1_{01}\rightarrow 0_{00}$, $1_{11}\rightarrow 0_{00}$, $2_{11}\rightarrow 2_{02}$, $2_{11}\rightarrow 2_{12}$, $2_{21}\rightarrow 2_{12}$, $3_{21}\rightarrow 3_{12}$, and $3_{31}\rightarrow 3_{22}$ rotational transitions, all in the 12 to 8 GHz range of our spectrometer, were investigated at zero field. The Zeeman studies were limited to the $J\rightarrow J'=1\rightarrow 0$ and $2\rightarrow 2$ transitions, which were all investigated under $\Delta M_J=0$ and $\Delta M_J=\pm 1$ selection rule. In Table 1 we present the experimental zero field frequencies of the hfs multiplets shown in Fig. 1, and in Table 2 we present the experimental satellite frequencies of the Zeeman pattern* shown in Figure 2.

* The complete list of frequencies can be obtained by D. H. Sutter at the address given at the beginning of this paper. It was also deposited under TNA 22 at the University of Kiel library.

For the theoretical background of the nuclear quadrupole coupling we refer to Chap. IX of [12]. The theoretical background of the molecular rotational Zeeman effect has been treated extensively in [13]. The zero field multiplet splittings were analyzed with our program SUZIQ.FOR (author O. Böttcher). In this program the matrix of the rigid rotor Hamiltonian, supplemented by the nulear quadrupole coupling and spin rotation coupling of up to three nuclei, is set up in the coupled basis. The following coupling scheme is used:

$$I_1+I_2=I_{12},\quad I_{12}+I_3=I_{123},\quad I_{123}+J=F,$$

where $(h/2\pi)\cdot I_i$ $(i=1, 2, 3)$ denote the spin angular momenta of the three nuclei, $(h/2\pi)\cdot J$ denotes the angular momentum associated wih the rotation of the molecule, and $(h/2\pi)\cdot F$ denotes the overall angular momentum including spins. Since matrix elements off-

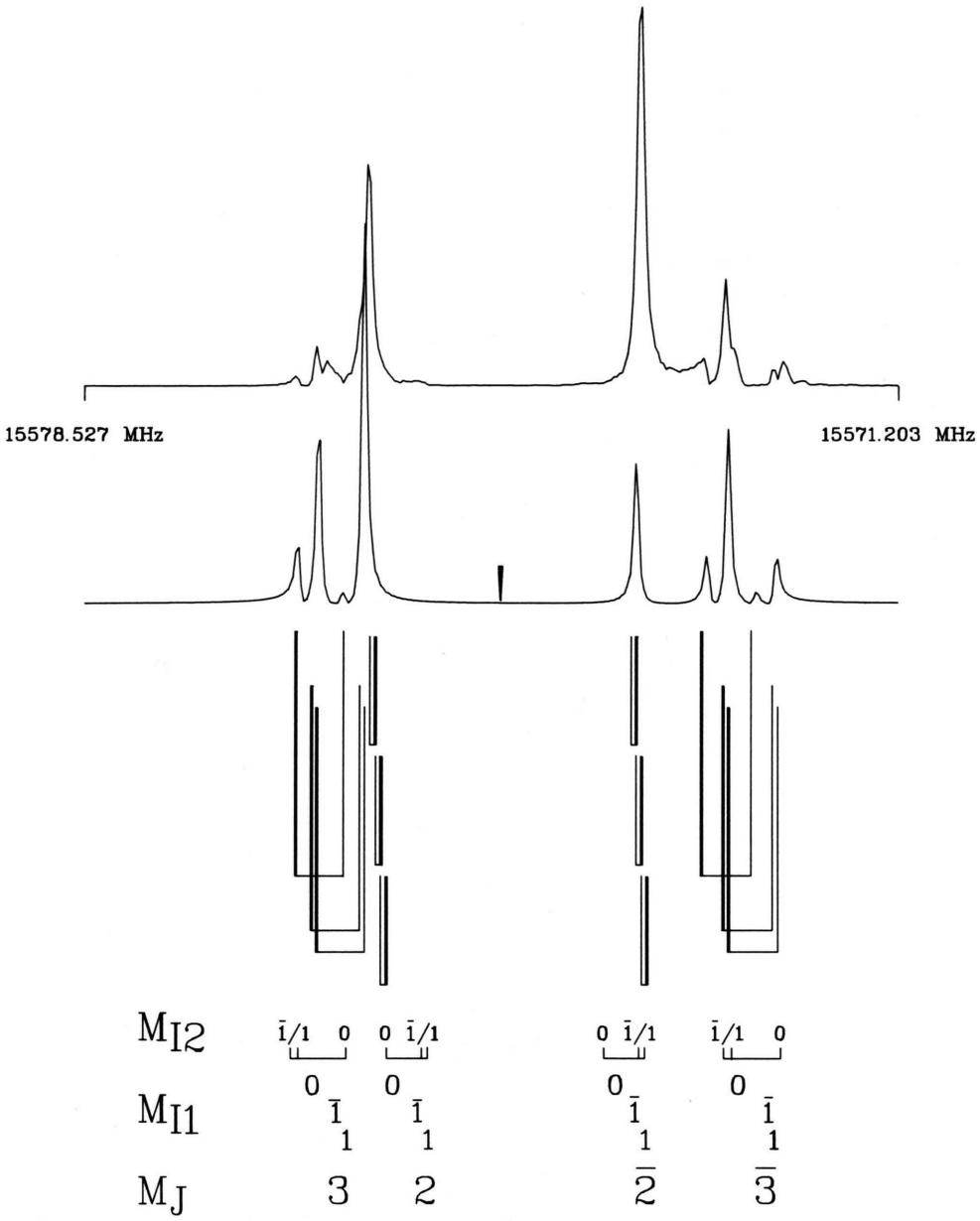

Fig. 2. Fourier transform power spectrum of the transient emissions from the Zeeman-hfs-pattern of the $3_{31}-3_{22}$ rotational transition observed under $\Delta M_J=0$ selection rule in a field of 16 032 Gauss (1.6032 Tesla). The lower trace shows the corresponding high power/short pulse simulation. The dagger indicates the hypothetical center frequency of the transition. Since the sample was polarized at a frequency 3.9 MHz below the center frequency, the differences between experiment and simulation are larger than in Figure 1. The bar pattern below shows the individual satellites marked by the magnetic quantum numbers of the overall rotation, M_J, and of the two nuclei M_{I_n} (index 1 for the pyrrolic, index 2 for the pyridinic nitrogen). A bar above a number indicates the negative sign. In the absence of nuclear quadrupole coupling, there would be only six satellites corresponding to $M_J=3, 2, 1, -1, -2, -3$ with relative intensities proportional to M_J^2, i.e. 9:4:1:1:4:9. Quadrupole coupling of the pyridinic nitrogen essentially leads to doublet splitting with intensity ratio 2 (for $M_{I2}=\pm 1$) to 1 ($M_{I2}=0$). Each of these satellites is further split into a narrower subdoublet due to the quadrupole coupling of the pyrrolic nitrogen. Since high-field uncoupling of spins and overall rotation is not yet complete, the $M_I=\pm 1$ satellites do not exactly coincide and the complete hfs pattern contains 54 satellites. Experimental conditions: Sample pressure: 2 mTorr, temperature: 298 K, pulse length: 100 ns, delay: 1000 ns, sample intervall: 10 ns, data points: 2048.

Table 2. Zeeman multiplet of the $3_{31} \rightarrow 3_{22}$ rotational transition of 1 D-pyrazole observed under $\Delta M_J = 0$ selection rule at a magnetic field strength of 16 032 Gauss. This transition is shown in Fig. 2, because of its comparatively uncomplicated multiplet structure. ν_{exp}: experimental splitting with respect to the hypothetical center frequency of the unsplit transition; ν_{calc}: splitting calculated from the optimized Zeeman parameters (Table 4), and quadrupole coupling constants (Table 3), $\delta\nu$: $\nu_{exp} - \nu_{calc}$.

M_J	M_{I1}	M_{I2}	M'_J	M'_{I1}	M'_{I2}	Frequency (MHz)			Intensity %
						ν_{exp}	ν_{calc}	$\delta\nu$	
$J_{K_aK_c} \rightarrow J'_{K_aK_c}$: $3_{31} \rightarrow 3_{22}$; ν_{center}: 15 574.801(6) MHz									
−3	−1	−1	−3	−1	−1	−2.044	−2.041	−0.003	3.9
−3	−1	0	−3	−1	0	−2.470	−2.470	0.000	3.9
−3	−1	1	−3	−1	1	−2.044	−2.055	0.011	3.9
−3	0	−1	−3	0	−1	−1.832	−1.859	0.027	3.9
−3	0	0	−3	0	0	−2.286	−2.288	0.002	3.9
−3	0	1	−3	0	1	−1.832	−1.873	0.041	3.9
−3	1	−1	−3	1	−1	−2.044	−2.043	−0.001	3.9
−3	1	0	−3	1	0	−2.470	−2.472	0.002	3.9
−3	1	1	−3	1	1	−2.044	−2.057	0.013	3.9
−2	−1	−1	−2	−1	−1	−1.235	−1.237	0.002	1.7
−2	−1	0	−2	−1	0	−1.235	−1.220	−0.015	1.7
−2	−1	1	−2	−1	1	−1.235	−1.237	0.003	1.7
−2	0	−1	−2	0	−1	−1.235	−1.238	0.003	1.7
−2	0	0	−2	0	0	−1.235	−1.221	−0.014	1.7
−2	0	1	−2	0	1	−1.235	−1.238	0.003	1.7
−2	1	−1	−2	1	−1	−1.235	−1.241	0.005	1.7
−2	1	0	−2	1	0	−1.235	−1.224	−0.011	1.7
−2	1	1	−2	1	1	−1.235	−1.241	0.005	1.7
2	−1	−1	2	−1	−1	1.213	1.216	−0.003	1.7
2	−1	0	2	−1	0	1.213	1.224	−0.011	1.7
2	−1	1	2	−1	1	1.213	1.216	−0.003	1.7
2	0	−1	2	0	−1	1.213	1.214	−0.001	1.7
2	0	0	2	0	0	1.213	1.222	−0.009	1.7
2	0	1	2	0	1	1.213	1.214	−0.001	1.7
2	1	−1	2	1	−1	1.213	1.213	0.000	1.7
2	1	0	2	1	0	1.213	1.221	−0.007	1.7
2	1	1	2	1	1	1.213	1.213	0.000	1.7
3	−1	−1	3	−1	−1	1.644	1.652	−0.007	3.9
3	−1	0	3	−1	0	1.213	1.229	−0.016	3.9
3	−1	1	3	−1	1	1.644	1.638	0.006	3.9
3	0	−1	3	0	−1	1.822	1.834	−0.012	3.9
3	0	0	3	0	0	1.401	1.411	−0.010	3.9
3	0	1	3	0	1	1.822	1.821	0.001	3.9
3	1	−1	3	1	−1	1.644	1.649	−0.005	3.9
3	1	0	3	1	0	1.213	1.226	−0.013	3.9
3	1	1	3	1	1	1.644	1.635	0.009	3.9

Table 3. Rotational constants and nuclear quadrupole coupling constants of pyrazole and 1 D-pyrazole. B_{aa}, B_{bb}, B_{cc}: rotational constants in MHz ([4], p. 406); $\chi_{aa}(N_i)$, $\chi_{bb}(N_i)$, $\chi_{cc}(N_i)$, $(i = 1, 2)$: ^{14}N nuclear quadrupole coupling constants in MHz ([5], and this work). The index i refers to the pyrrolic $(i = 1)$ and the pyridinic nitrogen nucleus $(u = 2)$, respectively. The scaling factor −4.00111 MHz/a.u. [19] was used to convert from the ab initio field gradients to the ^{14}N quadrupole coupling constants. Uncertainties (in brackets) are single standard deviations of the least squares fit and are given in units of the least significant digit(s). The experimental $\chi_{ab}(N_i)$-values were deduced from the changes in the $\chi_{aa} - \chi_{bb}$ values upon deuteration.

	Pyrazole		1 D-pyrazole	
	Exper.	SCF	Exper.	SCF
B_{aa}	9618.770(13)		9455.230(5)	
B_{bb}	9412.535(13)		8859.733(5)	
B_{cc}	4755.853(13)		4572.874(4)	
χ_{aa}(N1)	1.391(6)	1.395	0.957(7)	0.979
χ_{bb}(N1)	1.662(6)	1.660	2.123(7)	2.083
χ_{cc}(N1)	−3.053(12)	−3.055	−3.082(6)	−3.062
χ_{ab}(N1)	−0.730(21)	−0.694	0.466(14)	0.441
χ_{aa}(N2)	−3.960(5)	−4.160	−0.507(9)	−1.291
χ_{bb}(N2)	3.140(5)	2.906	−0.378(9)	0.036
χ_{cc}(N2)	0.820(10)	1.254	0.885(9)	1.255
χ_{ab}(N2)	−1.943(6)	−2.610	4.046(5)	4.342

diagonal in the rotational quantum numbers J and K_aK_c are neglected in the program, its use is limited to nuclei such as ^{14}N or D considered here, with couplings sufficiently small as compared to energy differences between adjacent rotational states. The progam also calculates relative electric dipole transition intensities. They are obtained from the direction cosine matrix elements subjected to the same unitary transformation which diagonalizes the effective Hamiltonian matrix (simplified by the above neglection of the matrix elements off-diagonal in the rotational quantum numbers).

Since the effects of spin-rotation coupling and of deuterium quadrupole coupling proved to be below our experimental resolution, they were neglected in the final analysis of observed hfs-multiplets. This means that only the spins of the two nitrogens, I_1 and I_2 (the pyrrolic nitrogen carries the label 1) were coupled to an intermediate spin, I_{12}, which in turn was coupled with J, to give the overal angular momentum in units of $(h/2\pi)$, F. This coupling scheme is also used to designate the initial and final states of the transitions shown in Fig. 1 and Table 1. Note that this scheme differs from the one adopted in the program Q2SIM.FOR, which we had used in our study of the parent species [5] and which leads to a different designation.

For the analysis of the Zeeman spectra, the Hamiltonian matrix was set up in the more appropriate uncoupled basis; $|J, K_aK_c, M_J\rangle|I_1, M_{I1}\rangle|I_2, M_{I2}\rangle$ with matrix elements as given in [14]. Here again all matrix elements off-diagonal in J, K_aK_c are neglected and for each rotational state the M_J, M_{I1}, M_{I2}-submatrix of rank $(2J+1)\cdot(2I_1+1)\cdot(2I_2+1)$ is diagonalized numerically with the corresponding transformation of the direction cosine elements for the calcu-

Table 4. Zeeman parameters of pyrazole and 1 D-pyrazole. Only the relative sign of the g values can be determined from the high field Zeeman study reported here [20], but the opposite choice of sign Eq. (3) would lead to a negative value for $\langle|c^2|\rangle$ which is clearly impossible. g_{xx} $(x=a, b, c)$ diagonal elements of the molecular g-tensor, $2\xi_{aa}-\xi_{bb}-\xi_{cc}$, $2\xi_{bb}-\xi_{cc}-\xi_{aa}$: anisotropies of the susceptibility tensor ([5], and this work), in 10^{-6} erg G^{-2} mole^{-1}.

	Pyrazole	1 D-pyrazole
g_{aa}	−0.0750(1)	−0.1178(2)
g_{bb}	−0.1253(1)	−0.0762(2)
g_{cc}	0.0635(1)	0.0608(2)
$2\xi_{aa}-\xi_{bb}-\xi_{cc}$	39.53(24)	52.69(32)
$2\xi_{bb}-\xi_{cc}-\xi_{aa}$	51.20(21)	39.32(29)

Table 5. Principal inertia axes coordinates of the atoms in pyrazole and 1 D-pyrazole as calculated from the r_s-structure shown in Table 4 of [4], p. 410. The c-coordinates are zero due to the observed polanarity of the nuclear frame.

Atom	Mass/amu	Pyrazole		1 D-pyrazole	
		a/Å	b/Å	a/Å	b/Å
N1	14.003074	0.3949	−1.0010	1.0239	−0.2139
N2	14.003074	1.1751	0.0990	0.5320	1.0418
C3	12.000000	0.3093	0.1095	−0.7877	0.8721
C4	12.000000	−1.0325	0.6566	−1.1450	−0.4982
C5	12.000000	−0.332	−0.7122	0.0540	−1.1660
H(C3)	1.007825	0.6799	2.1222	−1.4312	1.7375
H(C4)	1.007825	−1.9299	1.2495	−2.1330	−0.9235
H(C5)	1.007825	−1.6781	−1.4906	0.2963	−2.2158
H(N1)	1.007825	0.8364	−1.8959		
D(N1)	2.014102			2.0113	−0.3352

lation of the relative intensities. Accordingly in Fig. 2 and Table 2 the satellites are designated by the quantum numbers, M_J, M_{I1} and M_{I2} of the corresponding upper and lower states, respectively. Since at fields above 10 kG (= 1 Tesla) uncoupling of spins and overall rotation is essentially complete $\Delta M_{I1}=0$ and $\Delta M_{I2}=0$ selection rules applied throughout our present investigation. For a discussion of the transition from the coupled basis of the uncoupled basis we refer to Chapt. IV of [13].

The least squares fit of the nuclear quadrupole coupling constants of the two ^{14}N nuclei and of the molecular g-tensor elements and magnetic susceptibility anisotropies to the zero field and high field multiplets was carried out in an iterative procedure as described earlier in [15]. Our results are presented in Table 3 (quadrupole coupling constants) and in Table 4 (g-tensor elements and susceptibility anisotropies). For later use we also give the rotational constants and the corresponding values for the parent species pyrazole.

Derived Molecular Parameters

The knowledge of the theoretical expressions for the g-tensor elements (compare Chap. IV of [13] for their rigorous derivation from first principles) made it possible to derive experimental values for the diagonal elements of the molecular electric quadrupole moment and for electronic ground state averages of the anisotropies in the second moments of the electronic charge distribution according to the equations

$$Q_{aa}=-\frac{h|e|}{16\pi^2 m_p}\left[\frac{2g_{aa}}{B_{aa}}-\frac{g_{bb}}{B_{bb}}-\frac{g_{cc}}{B_{cc}}\right]-\frac{2mc^2}{|e|N_A}(2\xi_{aa}-\xi_{bb}-\xi_{cc}), \quad (1)$$

$$\langle 0|\sum_i a_i^2-b_i^2|0\rangle=\sum_n Z_n(a_n^2-b_n^2)-\frac{h|e|}{8\pi^2 m_p}\left[\frac{g_{aa}}{B_{aa}}-\frac{g_{bb}}{B_{bb}}\right]+\frac{4mc^2}{3e^2N_A}[(2\xi_{aa}-\xi_{bb}-\xi_{cc})-(2\xi_{bb}-\xi_{cc}-\xi_{aa})]. \quad (2)$$

(and cyclic permutations).

The notation is as follows: h: Planck's constant, m: electron mass, m_p: proton mass, c: velocity of light, e: electron charge, Z: nuclear charge, N_A: Avogadro's constant, B_{aa}, B_{bb}, B_{cc}: rotational constants, a, b, c: principal inertia axes coordinates of the nuclei (index n) and electrons (index i).

The coordinates for the nuclei which enter into the expression for the anisotropies, were taken from the microwave substitution structure (r_s-structure) determined by the Kopenhagen group (Tables 3, 4 of [4], Table 5 in this work). In [13] we have argued that (1) and (2) with equilibrium coordinates for the nuclei should lead to values very close to the vibronic ground state averages. In order to account for the slight differences between the substitution structure and the equilibrium structure, an uncertainty of 0.1 Å^2 was assumed for the sums running over the nuclear coordinates in (2). Our quadrupole moments and our anisotropies in the second moments of the electronic charge distribution are given in Table 6.

Table 6. The sum of the squares of the nuclear coordinates multiplied by the atomic number, $\Sigma Z_n g_n^2$ ($g=a, b, c$) in Å^2; electronic ground state expectation values of the sum of the squares of the electron coordinates, $\langle|g^2|\rangle$ ($g=a, b, c$) in Å^2; anisotropies in the second moments of the electron charge distribution, $\langle|g^2-g'^2|\rangle$ ($g, g'=a, b, c, g\neq g'$) in Å^2; components of the molecular electric quadrupole moment tensors Q_{gg} ($g=a, b, c$) in 10^{-26} esu cm^2; bulk susceptibility (ξ_{bulk}) according to Haberditzl (a) and SCF-calculation (b) in 10^{-6} erg G^{-2} mole^{-1}; diagonal elements of the molecular magnetic susceptibility tensors, ξ_{gg} ($g=a, b, c$) in 10^{-6} erg G^{-2} mol^{-1} for pyrazole and 1 D-pyrazole. a) These values were calculated with the approximate bulk susceptibility according to the Haberditzl scheme (Table 7); b) these values were calculated using the $\langle|c^2|\rangle$-value of the "Gaussian 86" program as additional input for the ξ_{bulk} calculation (compare text) and *, the values were calculated using the $\langle|a^2|\rangle$-, $\langle|b^2|\rangle$-, $\langle|c^2|\rangle$-values of the "Gaussian 86" program with an assumed uncertainty of 0.2 Å^2 each, together with the experimental diagonal elements of the g-tensor (i.e. the susceptibilities were calculated from (3)).

	Pyrazole			1 D-pyrazole		
	Experimental		SCF+g	Experimental		SCF+g
$\Sigma Z_n a_n^2$		30.66(10)			31.66(10)	
$\Sigma Z_n b_n^2$		31.98(10)			31.02(10)	
$\Sigma Z_n c_n^2$		0.00(10)			0.00(10)	
$\langle\|a^2\|\rangle$	a)	37.10(24)	37.00(20)	a)	36.78(25)	36.57(20)
$\langle\|b^2\|\rangle$	a)	36.57(24)	36.34(20)	a)	37.05(25)	36.86(20)
$\langle\|c^2\|\rangle$	a)	6.81(24)	6.74(20)	a)	6.68(25)	6.74(20)
$\langle\|a^2-b^2\|\rangle$		0.53(20)	0.66(28)		−0.25(21)	−0.29(28)
$\langle\|b^2-c^2\|\rangle$		29.76(21)	29.60(28)		30.37(22)	30.11(28)
$\langle\|c^2-a^2\|\rangle$		−30.29(21)	−30.25(28)		−30.12(22)	−29.82(28)
Q_{aa}		−3.56(16)	−3.48(30)		5.84(22)	6.79(31)
Q_{bb}		9.79(14)	11.68(29)		−0.58(21)	−0.09(31)
Q_{cc}		−6.25(27)	−6.59(57)		−5.27(38)	−6.70(59)
ξ_{bulk}	a)	−44.95(50)	−43.92(68)*	a)	−44.95(50)	−43.92(68)*
	b)	−44.38(67)		b)	−46.13(86)	
ξ_{aa}	a)	−31.77(58)	−30.82(67)*	a)	−27.39(61)	−26.74(67)*
	b)	−31.20(65)		b)	−27.90(71)	
ξ_{bb}	a)	−27.88(57)	−27.01(67)*	a)	−31.75(60)	−30.81(67)*
	b)	−27.31(64)		b)	−32.35(72)	
ξ_{cc}	a)	−75.20(65)	−73.94(70)*	a)	−75.72(70)	−74.21(70)*
	b)	−74.62(72)		b)	−76.13(115)	

If the experimental values for the magnetic susceptibility anisotropies can be supplemented by a reliable value for the bulk susceptibility, $\xi_{\text{bulk}}=(\xi_{aa}+\xi_{bb}+\xi_{cc})/3$, the diagonal elements ξ_{aa}, ξ_{bb} and ξ_{cc} may be obtained individually. Then their knowledge also makes it possible to derive the electronic ground state expectation values for the electronic second moments according to (3) (see Chapt. II.A of [13]):

$$\langle|a^2|\rangle=\sum_n Z_n a_n^2+\frac{h}{16\pi^2 m_p}\left[\frac{g_{aa}}{B_{aa}}-\frac{g_{bb}}{B_{bb}}-\frac{g_{cc}}{B_{cc}}\right] \quad (3)$$

$$+\frac{2mc^2}{e^2 N_A}(\xi_{aa}-\xi_{bb}-\xi_{cc}) \text{ (and cyclic permutations).}$$

Unfortunately there was no experimental value for the bulk susceptibility available to us. We therefore proceeded as follows.

First we used Haberditzl's additivity scheme [16] to predict ξ_{bulk} from tabulated atomic core and bond contributions. The essence of this calculation is presented in Table 7. The result was $\xi_{\text{bulk}}(\text{pyrazole})=-44.95(50)\cdot 10^{-6}$ erg G^{-2} mole^{-1}. Haberditzl proposes to use an uncertainty of 1–2% for the bulk susceptibility value determined that way. Second we used the $\langle|c^2|\rangle$ analogue of (3) with an ab initio value for $\langle|c^2|\rangle$, the r_s-structure for the nuclear frame and the experimental value for the g-tensor elements and rotational constants and solved for $(\xi_{aa}-\xi_{bb}-\xi_{cc})$. From this linear combination of susceptibilities and from the experimental susceptibility anisotropies one can also obtain the bulk susceptibility and the individual components ξ_{aa}, ξ_{bb}, χ_{cc}. The $\langle|c^2|\rangle$-analogoue of (3) was used, rather than $\langle|a^2|\rangle$, since it is less susceptible to uncertainties in the nuclear configuration. To get an ab initio self consistent field value for $\langle|c^2|\rangle$ we did run the "Gaussian 86" program of Pople and coworkers [17] at the microwave r_s-structure. The 6-311 G** basis (triple zeta with polarization, p-orbitals at hydrogen and d-orbitals at carbon and nitrogen) was used in this calculation. The result

Table 7. Excerpt of the Haberditzl additivity scheme which we have used to calculate the bulk susceptibility of pyrazole and 1 D-pyrazole. For small molecules an error of 1–2% of the bulk susceptibility is assumed, compare too [16], pp. 38, 90, 97. A number as index denotes the number of non-hydrogen atoms, which are bonded to the atom. The index $(^+)$ corresponds to the sp^2-hybridisation of the atom and the index π is used for the contribution of the π-bond. All contributions to ξ_{bulk} are given in 10^{-6} erg G^{-2} mole^{-1}.

Core	3 C	−0.45
	4 H	−0.00
	2 N	−4.80
Bond increment	$3\ C_2^+-H$	−9.60
	$1\ N_2-H$	−1.80
	$2\ C_2^+-C_2^+$	−4.80
	$1\ C_2^+-N_2^+$	−1.50
	$1\ C_2^+-N_2$	−1.90
	$1\ N_2^+-N_2$	−2.20
	$1\ C_{2\pi}\ C_2$	−2.20
	$1\ C_{2\pi}\ N_2$	−2.00
Aromaticity exaltion		−13.70

was $\langle|c^2|\rangle = 6.747$ Å^2. For the subsequent Gaussian error propagation analysis we assumed an uncertainty of ± 0.2 Å^2 uncertainty in this $\langle|c^2|\rangle$-value.

Dependent on the isotopomer, two sets of ξ-values and two bulk susceptibilities were obtained that way. We present them in units of 10^{-6} erg G^{-2} mole^{-1}:

Pyrazole:

$\xi_{bulk} = -44.38(67)$, $\xi_{aa} = -31.20(65)$,
$\xi_{bb} = -27.31(64)$, $\xi_{cc} = -74.62(72)$.

1-pyrazole:

$\xi_{bulk} = -45.46(86)$, $\xi_{aa} = -27.90(71)$,
$\xi_{bb} = -32.35(72)$, $\xi_{cc} = -76.13(115)$.

Neglecting the very small effect of slightly different zero point averages, ξ_{cc} and ξ_{bulk} should be identical for both isotopomers. (The changes in ξ_{aa} and ξ_{bb} upon deuteration give information on the off-diagonal element ξ_{ab} (see below)). Indeed ξ_{cc} and ξ_{bulk} agree for both isotopomers within their uncertainty limits. Furthermore, the bulk value predicted within the Haberditzl additivity scheme, i.e. $-44.95 \cdot 10^{-6}$ erg G^{-2} mole^{-1}, closely agrees with the average of the values determined by the "$\langle|c^2|\rangle$-method". We therefore used the Haberditzl-bulk value to derive the individual second electronic moments and susceptibilities. The results are presented in Table 6.

The Complete Tensors of the Nitrogen Nuclear Quadrupole Coupling, χ_{N1} and χ_{N2}, the Molecular Magnetic Susceptibility, ξ, and the Molecular Electric Quadrupole Moment, Q

The complete tensors including their orientation and their otherwise not easily accessibly off-diagonal elements can be derived from their changes upon deuteration. We first treat quadrupole coupling and magnetic susceptibility, since they do not depend on the origin of the coordinate system within the molecule. Due to the symmetry plane there is only one non vanishing off-diagonal element, T_{ab} (where T stands for χ_{N1}, χ_{N2}, or ξ, respectively). Then if x and y designate the principal axes of the tensor under consideration, its aa- and bb-elements are related to its principal elements T_{xx} and T_{yy} through (compare too Figure 3)

$$T_{aa} = \cos^2(\measuredangle ax)\, T_{xx} + \cos^2(\measuredangle ay)\, T_{yy}$$
$$= \cos^2(\alpha)\, T_{xx} + \sin^2(\alpha)\, T_{yy}, \quad (4)$$

$$T_{bb} = \cos^2(\measuredangle bx)\, T_{xx} + \cos^2(\measuredangle by)\, T_{yy}$$
$$= \sin^2(\alpha)\, T_{xx} + \cos^2(\alpha)\, T_{yy} \quad (5)$$

with a corresponding set of equations for the deuterated (primed) species. Within the rigid rotor approximation T_{xx} and T_{yy} are the same for both species, and the changes from T_{aa} to $T_{a'a'}$ and from T_{bb} to $T_{b'b'}$ are due to the change from α to $\alpha' = \alpha + \delta$, where δ is calculated as 58.89° from the rotational constants of the parent species and the deuterated species (Table 3) as proposed by Rudolph (see (26) of [18]). Since the sum of the diagonal elements of the tensor is invariant under rotations, the essential information is contained in the differences

$$T_{aa} - T_{bb} = \cos(2\alpha) \cdot (T_{xx} - T_{yy}), \quad (6)$$

$$T_{a'a'} - T_{b'b'} = \cos(2\alpha + 2\delta) \cdot (T_{xx} - T_{yy}). \quad (7)$$

These differences are directly determined in the experiment. (In the case of the susceptibility, $\xi_{aa} - \xi_{bb}$ is obtained as $((2\xi_{aa} - \xi_{bb} - \xi_{cc}) - (2\xi_{bb} - \xi_{aa} - \xi_{cc}))/3\}$. Use of the cosine additivity rule and solving for α than leads to

$$\alpha = 0.5 \cdot \mathrm{Arctan}\left(\frac{\cos(2\delta)}{\sin(2\delta)} - \frac{1}{\sin(2\delta)} \cdot \frac{T_{a'a'} - T_{b'b'}}{T_{aa} - T_{bb}}\right). \quad (8)$$

Insertion of this value into (6) or (7) then leads to the difference $T_{xx} - T_{yy}$. Comparison with $T_{xx} + T_{yy}$ (directly measured as $-T_{cc}$ in the case of quadrupole

Table 8. Compilation of the elements of the ^{14}N nuclear quadrupole coupling tensors ($\chi_{qq}(N_l)$, $q=x, y, z$; $l=1, 2$) in MHz, the elements of the magnetic susceptibility tensor, (ξ_{qq}, $q=x, y, z$) in 10^{-6} erg G^{-2} mole^{-1}, and the elements of the molecular quadrupole tensor Q_{qq} ($q=x, y, z$) in 10^{-26} esu cm^2 each in its own principal inertia axes system. Also given are the off-diagonal elements of these tensor in the principal inertia axis system of pyrazole and 1 D-pyrazole. $\sphericalangle x, a$ are the angles between the a-axes of the molecular principal inertia system and the x-axis of the principal axis system of the tensor. *: as in Table 6.

	Pyrazole	1 D-pyrazole	Pyrazole	1 D-pyrazole
	Experimental		SCF-calculation	
$\chi_{xx}(N_1)$	0.791(36)		0.823	
$\chi_{yy}(N_1)$	2.277(29)		2.235	
$\chi_{zz}(N_1)$	−3.068(9)		−3.059	
$\sphericalangle x, a$	39.74° (15)	−19.14° (15)	39.59°	−19.30°
χ_{ab}	−0.730 (22)	0.460 (14)	−0.694	0.441
$\chi_{xx}(N_2)$	−4.473(10)		−5.020	
$\chi_{yy}(N_2)$	3.621(4)		3.765	
$\chi_{zz}(N_2)$	0.853(10)		1.255	
$\sphericalangle x, a$	14.35° (4)	−44.54° (5)	18.23°	−40.66°
$\chi_{ab}(N_2)$	−1.943(6)	4.046(5)	−2.610	4.342
ξ_{xx}	−32.17(86)		−31.15(87)*	
ξ_{yy}	−27.27(44)		−26.54(40)*	
ξ_{zz}	−75.41(68)		−74.07(70)*	
$\sphericalangle x, a$	−18.76° (661)	−77.65° (661)	17.08° (802)*	75.97° (802)*
ξ_{ab}	1.49 (56)	1.02 (56)	1.29 (57)	1.08 (57)*
Q_{xx}	−3.78(35)		−4.24	
Q_{yy}	9.60(8)		10.92	
Q_{zz}	−5.82(34)		−6.68	
$\sphericalangle x, a$	−0.39° (78)	−59.27° (78)	−0.16°	58.73°
Q_{ab}	0.08 (18)	5.88 (13)	1.48	5.95

coupling and indirectly determined with ξ_{bulk} as additional input, in the case of the susceptibility tensor) then leads to the final values given in Table 8 and illustrated in Figure 3. The off-diagonal elements, T_{ab}, then follow from T_{xx}, T_{yy} and α as

$$T_{ab}=0.5\sin(2\alpha)\cdot(T_{xx}-T_{yy})\,. \tag{9}$$

Unlike the $\chi_{N1,2}$ and ξ tensors the tensor of the molecular electric quadrupole moment, Q, also depends on the location of the reference system within the molecule, if the molecule has a nonvanishing electric dipole moment. However, this case can be reduced to the case treated before. To this end we introduce an intermediate reference system a'', b'', c'' with its origin already at the center of mass of the deuterated species but with its axes still parallel to the a, b, and c-axes of the parent species. From the general expression for the quadrupole moments with respect to this intermediate system,

$$Q_{a''a''}=0.5\cdot|e|\left[\sum_n Z_n(2a_n''^2-b_n''^2-c_n''^2)-\langle 0|\sum_i 2a_i''^2-b_i''^2-c_i''^2|0\rangle\right], \tag{10}$$

and with $a_j''=a_j-\Delta a$, $b_j''=b_j-\Delta b$, $c_j''=c_j$ (j=nuclear or electronic label; Δa, Δb=coordinates of the center of mass of the deuterated species with respect to the principal intertia axes system of the parent species) we get

$$\begin{aligned}Q_{a''a''}&=Q_{aa}-2\Delta a\,\mu_a+\Delta b\,\mu_b,\\ Q_{b''b''}&=Q_{bb}-2\Delta b\,\mu_b+\Delta a\,\mu_a,\\ Q_{c''c''}&=Q_{cc}+\Delta a\,\mu_a+\Delta b\,\mu_b,\end{aligned} \tag{11}$$

with μ_a, μ_b: dipole moments of pyrazole.

Then Q_{aa} and Q_{bb} can be used in place of $T_{a'a'}$ and $T_{b'b'}$ and the subsequent derivation is as given before. For this calculation we used $\Delta a=0.013$ Å and $\Delta b=-0.027$ Å as calculated from the r_s-structure and the dipole moment components of pyrazole as determined by Kirchhoff [1] ($|\mu_a|=1.640(13)$ D, $|\mu_b|=1.488(21)$ D) with the signs given by the SCF calculation. (At the r_s-structure and with the 6-311 G** basis, the "Gaussian 86" program calculates $\mu_a=-1.747$ D and $\mu_b=+1.638$ D). Our results for the molecular electric quadrupole moment are given at the bottom of Table 8 and in Figure 3.

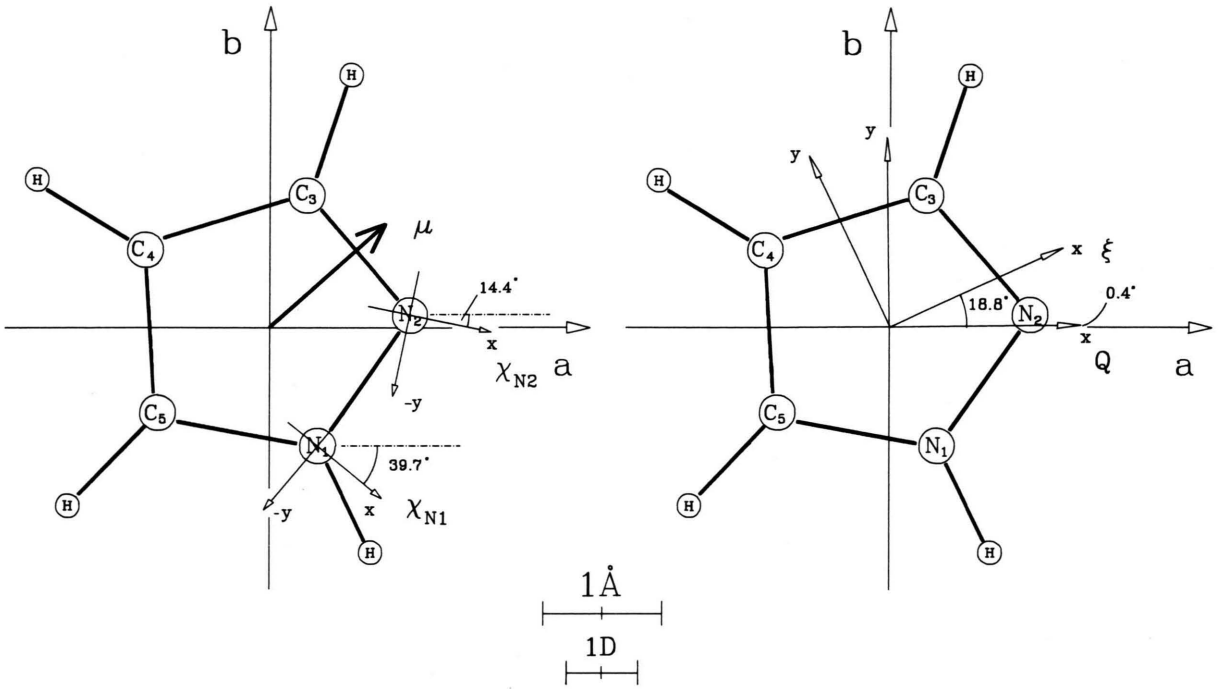

Fig. 3. Experimental results for the tensor orientations in pyrazole, ^{14}N nuclear quadrupole tensors, χ, at left, magnetic susceptibility, ξ, and molecular electric quadrupole moment, Q, at right. The orientation of the electric dipole moment, μ [1], is also shown for comparison.

Discussion

We restrict our discussion to the comparison of the experimental results for the second electronic moments, for the molecular electric quadrupole moment tensor and for the ^{14}N nuclear quadrupole coupling tensor with the ab initio results of the "Gaussian 86" SCF calculation carried out for the microwave r_s-structure (see Table 5). Table 6 shows that the electronic second moments $\langle|a^2|\rangle$ etc. and the molecular electric quadrupole moments calculated from the SCF-wavefunction are already in fair agreement with the experimental values. (Note that the single standard deviations are given as uncertainties in the experimental values.) As far as the ^{14}N quadrupole coupling tensors are concerned, the situation is less satisfactory. First of all, the conversion factor used to calculate the quadrupole coupling constants from the electric feld gradients at the nuclei under consideration corresponds to a value of only about 17 mbarn for the ^{14}N nuclear quadrupole moment rather than the experimental value of 19.3 mbarn published by Winter and Andrä [21]. Second, while this conversion factor leads to a very pleasing prediction of the pyrrolic quadrupole coupling tensor, the prediction for the pyridinic quadrupole coupling tensor is considerably off if compared with the experimental values. Also a separate down scaling of the electronic contribution to the electric field gradients at the ^{14}N nuclei, to roughly 93% of their ab initio values [22], which appeared to us as a useful method for compensation of possibly systematic errors in the electronic wavefunction does not lead to a satisfactory result in the present case. We therefore have initiated a systematic study of quadrupole coupling constants for sp^2-hybridized ^{14}N nuclei, both experimentally and quantum chemically at our laboratory.

Acknowledgements

The support from Deutsche Forschungsgemeinschaft and Fonds der Chemischen Industrie is gratefully acknowledged. We also would like to thank Prof. Dr. H. Dreizler for critically reading the manuscript. The ab initio calculations were performed on the CRAY-system of the Rechenzentrum der Universität Kiel.

[1] W. H. Kirchhoff, J. Amer. Chem. Soc. **89,** 1312 (1967).
[2] G. C. Blackman, R. D. Brown, and F. R. Burden, J. Mol. Spectrosc. **36,** 528 (1971).
[3] G. C. Blackman, R. D. Brown, F. R. Burden, and A. Mishra, J. Mol. Struct. **9,** 465 (1971).
[4] L. Nygaard, D. Christen, J. T. Nielsen, E. J. Pedersen, O. Snerling, E. Vestergaard, and G. O. Sorensen, J. Mol. Struct. **22,** 401 (1974).
[5] M. Stolze and D. H. Sutter, Z. Naturforsch. **42a,** 49 (1987).
[6] O. Böttcher, B. Kleibömer, and D. H. Sutter, Ber. Bunsenges. Phys. Chem. **93,** 207 (1989).
[7] U. Andresen and B. Kleibömer, Rev. Sci. Instrum. **59,** 1088 (1988).
[8] B. Kleibömer and D. H. Sutter, Z. Naturforsch. **43a,** 561 (1988).
[9] L. Albinus, J. Spieckermann, and D. H. Sutter, J. Mol. Spectrosc. **133,** 128 (1989).
[10] H. Dreizler, Mol. Phys. **59,** 1 (1986).
[11] J. Haekel and H. Mäder, Z. Naturforsch. **43a,** 203 (1988).
[12] W. Gordy and R. L. Cook, Microwave Molecular Spectra, 3rd ed., John Wiley, New York 1984.
[13] D. H. Sutter and W. H. Flygare, Topics in Current Chem. **63,** 89 (1976).
[14] K. F. Dössel and D. H. Sutter, Z. Naturforsch. **34a,** 469 (1979).
[15] O. Böttcher, N. Heineking, and D. H. Sutter, Z. Naturforsch. **44a,** 655 (1989).
[16] W. Haberditzl, S.B. Deutsch. Akad. Wiss. Berlin, Akademie-Verlag, Berlin 1964, p. 1–100.
[17] "Gaussian 86": M. J. Frisch, J. S. Binkley, H. B. Schlegel, K. Raghavachari, C. F. Melius, R. L. Martin, J. J. P. Stewart, F. W. Bobrowicz, C. M. Rohlfing, L. R. Kahn, D. J. Defrees, R. Seeger, R. A. Whiteside, D. J. Fox, E. M. Flender, and J. A. Pople, Carnegie-Mellon Quatum Chemistry, Publishing Unit, Pittsburgh PA 1984.
[18] H. D. Rudolph, J. Mol. Spectrosc. **89,** 430 (1981).
[19] H. Krause, D. H. Sutter, and M. H. Palmer, Z. Naturforsch. **44a,** 1063 (1989).
[20] M. Stolze and D. H. Sutter, Z. Naturforsch. **40a,** 998 (1985).
[21] H. Winter and H. J. Andrä, Phys. Rev. **A 21,** 581 (1980).
[22] A. Klesing and D. H. Sutter, Z. Naturforsch. **45a,** 817 (1990).